



Spatial and orientation patterns of experimental stone tool refits

Ignacio de la Torre¹ · Nils Vanwezer^{1,2} · Alfonso Benito-Calvo³ · Tomos Proffitt¹ · Rafael Mora⁴

Received: 15 March 2018 / Accepted: 7 September 2018 / Published online: 20 September 2018
© The Author(s) 2018

Abstract

Freehand and bipolar experimental knapping of quartzite from Olduvai Gorge in Tanzania is used to conduct spatial analysis of artefact distributions using GIS techniques, and to investigate the orientation of refit lines using circular histograms. The aim of our study is to discern patterns that can be applied to the archaeological record in two domains, namely the identification of knapping episodes and the utility of refitting line orientations in addressing post-depositional disturbance. Our spatial analysis shows that distinctive clustering patterns can be discerned according to knapping stance, handedness and flaking technique. The circular dispersion of refit lines in the horizontal distribution of bipolar assemblages is strongly patterned, indicating that anisotropy of conjoining sets is inherent to pristine hammer-and-anvil knapping episodes.

Keywords Conjoining sets · Quartzite · Bipolar flaking · GIS · Circular histograms · Olduvai Gorge

Introduction

The study of spatial distributions in experimental lithic scatters covers a range of topics, including knapper handedness (Bargalló et al. 2017), knapper stance (Newcomer and de Sieveking, 1980; Barton and Bergman 1982; Schick 1984; Fischer 1990; Kvamme 1997), reduction strategy and raw material (Kvamme 1997), hammer type (Newcomer and de Sieveking, 1980; Kvamme 1997) and post-depositional processes (Bowers et al. 1983; Gifford-González et al. 1985; Schick 1984; Nielsen 1991; Texier et al. 1998; Lenoble et al. 2008; Bertran et al. 2015; Driscoll et al. 2016). These studies have produced relevant observations on the spatial distribution of experimental scatters, but quantitative results based on systematic GIS analyses are yet to be done. Such lack of

quantification in experimental assemblages applies both to density patterns and the refitting of the lithic sets produced.

Analysis of orientation patterns in archaeology is traditionally linked to the study of post-depositional processes (e.g. Isaac 1967; Schick 1984; Kreutzer 1988; Pope 2002; Lenoble and Bertran 2004; Boschian and Saccà, 2010; Benito-Calvo and de la Torre 2011; Benito-Calvo et al. 2009, 2011; Sánchez-Romero et al. 2016; de la Torre and Wehr 2018; McPherron 2018), and refitting is widely recognised as a powerful tool to disentangle site formation (e.g. Cahen 1980; Villa 1982, 2004; Hofman 1986; Bordes 2003; Deschamps and Zilhão, 2018). Nonetheless, most studies concerned with taphonomic processes have addressed the vertical dimension of conjoining sets and their stratigraphic implications, while the horizontal dimension has received less attention in archaeological (e.g. Austin et al. 1999; Pope 2002; Ashton et al. 2005; Sisk and Shea 2008; Santamaría et al. 2010; de la Torre et al. 2014; Deschamps and Zilhão, 2018) and experimental (e.g. Schick 1984) assemblages.

This paper aims to contribute to the literature by exploring spatial dynamics of experimental knapping episodes and conclusions that can be drawn from the orientation patterns of refits. The baseline distribution for artefact and refit orientations is often assumed to be random, with the assumption that any variation is the product of natural processes. While that is certainly the case for the orientation of the long axes of items (Toots 1965; Nagle 1967; Wendt 1995), and it is not realistic to envisage undisturbed assemblages where artefact and bone

✉ Ignacio de la Torre
i.torre@ucl.ac.uk

¹ University College London, Institute of Archaeology, 31-34 Gordon Square, WC1H 0PY, London, UK

² Max Planck Institute for the Science of Human History, Kahlaische Strasse 10, 07745 Jena, Germany

³ CENIEH, Paseo Sierra de Atapuerca, 3, 09002 Burgos, Spain

⁴ Centre d'Estudis del Patrimoni Arqueològic de la Prehistòria, Facultat de Lletres, Universitat Autònoma de Barcelona, 08193 Bellaterra, Spain

axes are preferentially oriented (de la Torre and Benito-Calvo 2013), there is no evidence to suggest this random patterning is inherent to other variables such as refit lines.

To address these issues, our work includes the study of refit orientation patterns and the spatial analysis of four knapping experiments on quartzite from Olduvai Gorge in Tanzania. The goal of these experiments was to recreate core-and-flake assemblages through freehand and bipolar knapping techniques. Our analysis involves refitting of all experimental sequences, digital mapping of the artefact distribution, spatial analysis of artefact clusters and analysis of the refit orientation patterns. Through this, the study aims to elucidate clustering patterns of experimental lithic scatters, and reflect on the validity of orientation data of refit sets for spatial analysis in Palaeolithic assemblages.

Materials and methods

This paper involves the study of four knapping experiments (named Exp. 18, Exp. 40, Exp. 54 and Exp. 56) with quartzite (sensu Hay 1976) sourced from the Naibor Soit hills at Olduvai Gorge, Tanzania, from a repository within the Lithics Laboratory at the Institute of Archaeology, University College London. The aim of these four experiments was to produce as many flakes from individual block blanks using simple freehand and bipolar knapping techniques.

Knapping

All experiments were performed by one of us (TP), a right-handed knapper with 9 years of knapping experience, over a 2×2 m square cloth laid on top of a tile floor in an enclosed outdoor space. Two of the experiments (Exp. 18 and 40) were conducted using freehand knapping, in which the core was held in the left hand and struck with the hammerstone in the right hand. Exp. 18 was performed standing with feet 80 cm apart, and in Exp. 40 the knapper was kneeling (Fig. 1). Both cores were rotated and flipped whenever angles on a plane became too obtuse, but platforms were not prepared. Knapping continued until the core lost suitable flaking angles. Obtained flakes were dropped from the height of the hand. Exhausted cores were placed on the floor below their knapping position.

The other two experiments (Exp. 54 and 56) involved bipolar knapping (Fig. 1). The cores were placed on top of the anvil and stabilised with the left hand, while the right hand struck with the hammerstone at a 90° angle to the platform. Both experiments were performed kneeling to reach the anvil, and once exhausted, cores were left in their flaking position on the anvil.

Mapping

Knapping sequences were videotaped, and the resulting experimental scatters were photographed from an orthogonal view as well as from multiple angles, with each photograph overlapping by at least 60%. The images were combined to create a high-resolution photo merge using Adobe Photoshop for Exp. 18, 40 and 56, and Agisoft PhotoScan for Exp. 54 (in this case a 3D photogrammetry model was first created and then a 2D orthophoto was extracted). The resulting plans were then used to map in situ the all pieces over 2 cm in size within the 2×2 m cloth. These pieces were given an individual ID and labelled with a QR code (Table 1). Smaller debris were collected per $0.5 \text{ m} \times 0.5 \text{ m}$ quadrants.

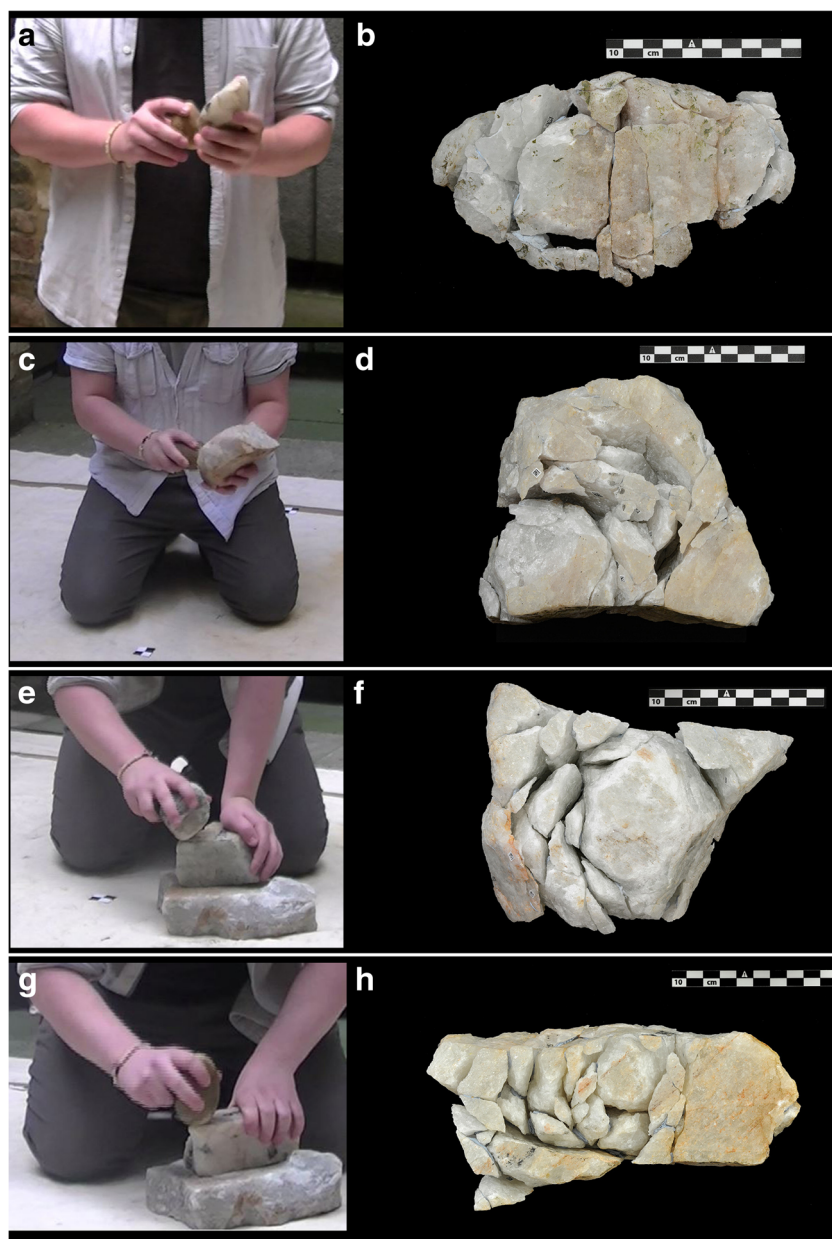
The photo maps of knapping scatters were imported into ArcGIS 10 as raster images and then georeferenced. The position of the knapper in each experiment was recorded and used as an arbitrary north. Polygon shapefiles were created along the outlines for each numbered piece and, where appropriate, the anvil. The centroid of each shapefile as designated by ArcGIS was used as the x, y coordinate for each piece.

Refitting

All material that received a unique identifier was measured (maximum length, width, thickness and weight), classified technologically and subjected to refit analysis. Refitting of Olduvai quartzite is notoriously difficult even in experimental settings (Proffitt and de la Torre 2014; Byrne et al. 2016), and thus the videos, images of the pre-modified blocks and photo maps were used to help identify the sequence position of certain pieces. Still, conjoining of freehand experiments took an average of 9 h each. Due to large amounts of crushing on the bipolar sequences, refitting was even more laborious in the case of Exp. 54 and 56, and took an average of 13 h each.

The analysis of refit sets was largely based on Czesla (1990) and De Loecker et al. (2003). The availability of videos, photogrammetry and the completeness of the assemblages enabled us to produce a more refined Harris Matrix for each refit set, in which each stage consists of a single flake or fragment set (i.e. refitting fragments resulting from a single strike) (Hiscock 1986), and to record the distance and orientation between successive flakes (section D in Figs. 2, 3, 4 and 5). Two additional options to represent refit lines were used to analyse the assemblages; one was to visualise all pieces as ‘projectiles’ originating from the core to show the spatial dispersion of the pieces (section B in Figs. 2, 3, 4 and 5). In addition, we produced maps with bi-directional refit lines between dorsal-ventral, transverse and longitudinal refits (section F in Figs. 2, 3, 4 and 5). Once such conjoining sequences were established for all four experiments, they were placed into an ArcGIS add-in module that we scripted to analyse refit sets spatially.

Fig. 1 Experimental refit sets studied in this paper. **a, b** Exp. 18, freehand standing. **c, d** Exp. 40, freehand kneeling. **e–h** Exp. 54 (**e, f**) and Exp. 56 (**g, h**), bipolar kneeling



Spatial analysis

Average nearest neighbour (ANN), Getis–Ord General G and Global Moran’s were applied to identify clustered, uniform or dispersed patterns. Ripley’s K Function was used to test if clustering changed over a range of distances and Global Moran’s I to establish the distance of maximum clustering. Identification of clusters was made using Getis–Ord G_i^* statistics (Sánchez-Romero et al. 2016). The quantitative variables used in G_i^* were frequency, weight and length of pieces, using the inverse Euclidean distance as the spatial relationship between artefacts. Getis–Ord and Global Moran’s statistics for frequency of artefacts followed the quadrat method, where counting of pieces was conducted in quadrats of 125 mm,

which is twice the size of the mean area per piece, considering the maximum area of dispersion for artefacts of all the experiments. Artefact frequency was also analysed through kernel density maps.

Orientation patterns

An add-in for ArcGIS was scripted to calculate distances between conjoining artefacts, and also orientation of the refit lines, based on trigonometric relationships on a Cartesian coordinate system. This script calculates both the direction and azimuth (where sequencing can be ascertained). The orientation data obtained with this ArcGIS module was then plotted into Rose diagrams with GeoRose software.

Table 1 Assemblage composition and main features of the refitted artefacts

			Exp. 18	Exp. 40	Exp. 54	Exp. 56
Assemblage composition*	Mapped	Total plotted artefacts	305	289	335	402
	Refitted	Complete flakes	29	27	24	18
		Flake fragments	7	21	17	27
		Total refitted artefacts**	37	49	42	46
Distance (mm)	Product to core	Mean	343	281	537	470
		Median	271	233	509	361
		Min	48	22	72	44
		Max	761	886	1162	1618
		SD	196	192	303	359
		Mean	385	293	475	467
	Between conjoining artefacts	Median	269	258	480	398
		Min	24	38	72	39
		Max	1216	978	970	1300
		SD	280	196	242	347

*Only artefacts larger than 20 mm. **Include the one core in each experiment refitting with flakes/flake fragments

The circular dispersion of displacement vectors was characterised using circular histograms and circular descriptive statistics (Fisher 1995). To estimate the reference direction of the assemblages, we used the mean direction (mean Cartesian vector unit) and the modal direction (the direction of maximum concentration of data). The module of the mean vector unit (R) was used as an index of dispersion (Benito-Calvo et al. 2009, 2011), varying between 1 (when all vector all coincident) and 0 (when the dispersion is high). Since R is not a useful indicator of data spreading unless they comprise unimodal distribution, we first combined a unimodal statistical test (Rayleigh's test) with omnibus tests (Rao's spacing, Watson's and Kuiper's tests) to corroborate that the data followed mainly a unimodal distribution (Benito-Calvo and de la Torre 2011; de la Torre and Benito-Calvo 2013). Concentration was also estimated using the concentration parameter K (Fisher 1995), which measures the departure of the distribution from a perfect circle (uniform distribution). Circular histograms in 15° (Figs. 2–5) and 5° (Fig. 8) bins and descriptive statistics were also calculated weighting the vectors and axis according to the distance between artefacts and to the weight of pieces. Statistics were calculated using Oriana 3.13 and SpheriStats 3.1.

Results

Spatial distribution of artefacts and refit lines

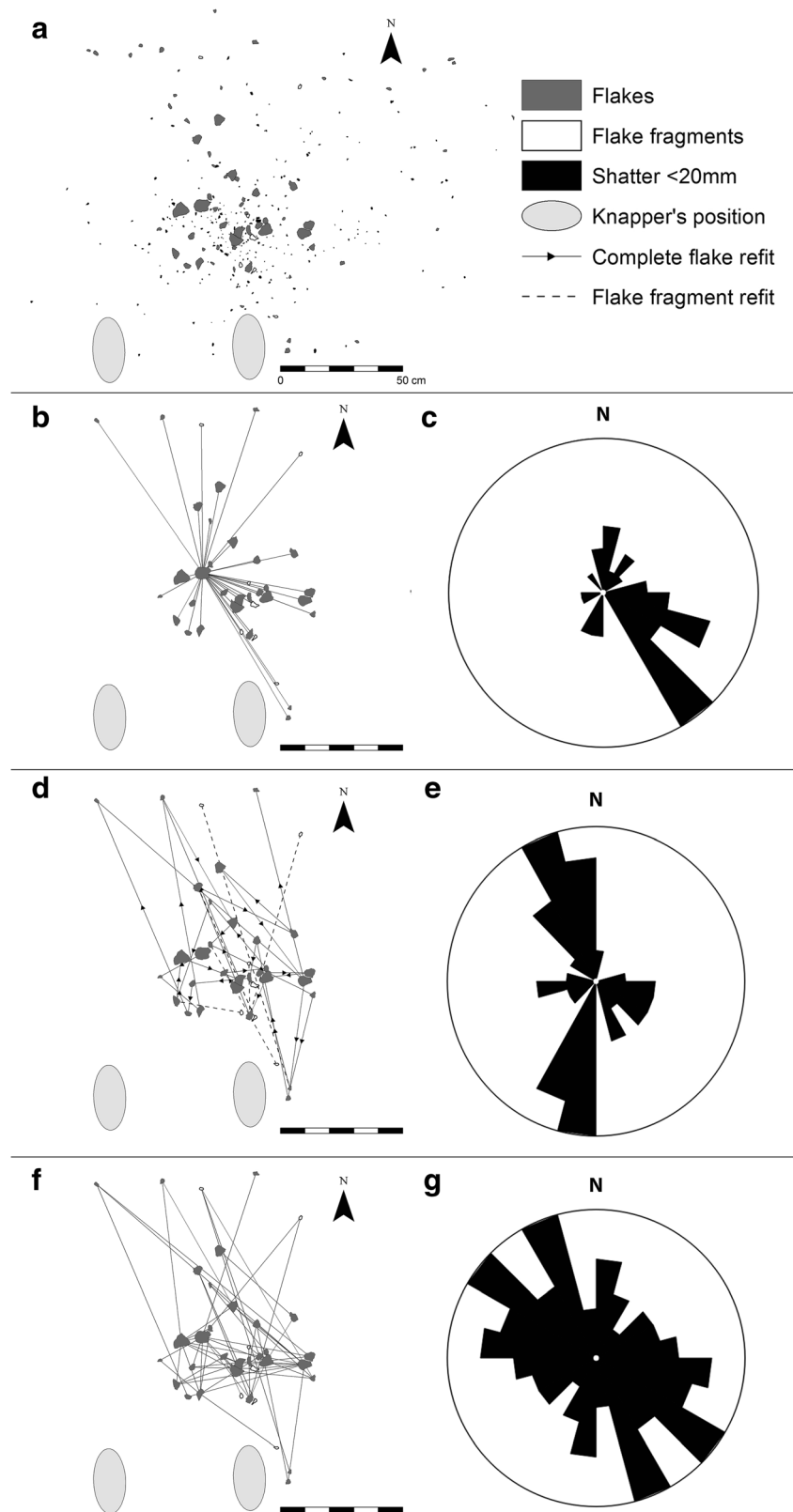
The Rose diagram of Exp. 18 shows that about half of the pieces are located within a 75° interval to the southeast of

the core (Fig. 2c), with the rest evenly distributed in all directions. The mean distance between products and the core is 343 mm, and the longest is 761 mm (Table 1). Analysis of the sequence (28 stages) shows that the majority of products landed to the northwest or south of the previous removal (Fig. 2e). More than 75% of the stages are less than 600 mm away from the preceding product (Fig. 6b). Refits have a mean distance of 385 mm (Table 1), and longer refit lines produce a largely elongated NW–SE trend (Fig. 2g).

Figure 3c shows that most artefacts in Exp. 40 occur in a 90° interval to the northeast of the core. More than 75% of core-product distances (Fig. 3b) are less than 400 mm, with outliers at 681 mm and 886 mm (Fig. 6a and Table 1). The knapping sequence (27 stages; Fig. 3d) shows a general trend of removals to move towards the east diagonally, and almost every other stage is to the North or South of its previous and next stage, forming a N–S trend (Fig. 3e). This is corroborated by the refit orientation circular histogram (Fig. 3g), which also indicates an additional trend from NE to SW. Many of the refits are less than 400 mm from one another (Fig. 6c), thus following the pattern of core–product distances.

In the case of Exp. 54, most pieces are within a 120° interval east from the core (Fig. 4c). Core–flake distances range between 72 and 1162 mm (Fig. 6a). There are 21 stages in the sequence, which shows an E–W trend (Fig. 4e). Most distances between successive stages are less than 600 mm, although there is a larger amount of variation in the lower end of the distribution than in free-hand experiments. The Rose diagram of refits (Fig. 4g) shows a strong unimodal pattern along the E–W axis.

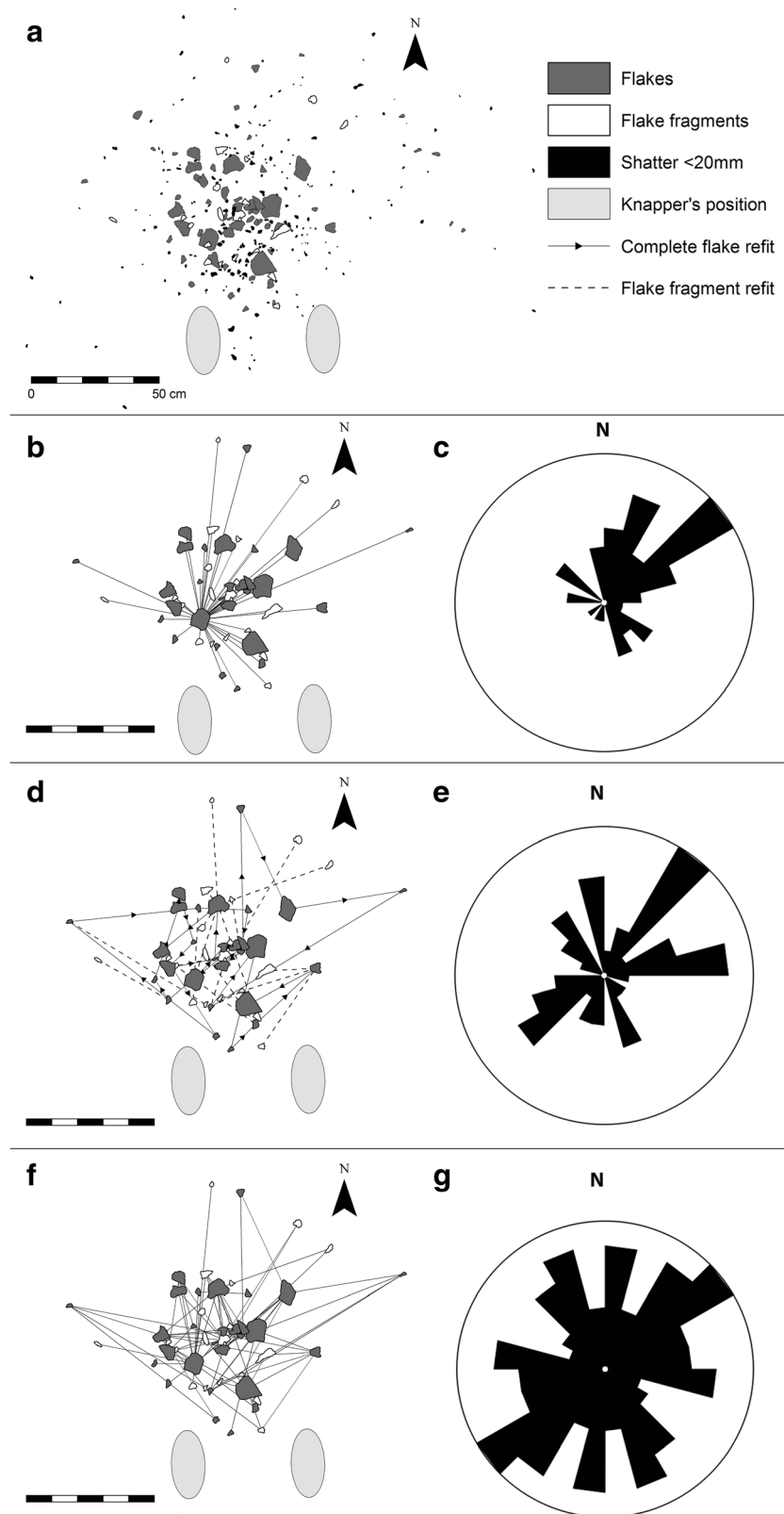
Fig. 2 Maps (a–b, d, f) and circular histograms (c, e, g) of Exp. 18. **a** All plotted artefacts. **b**, **c** Distribution of refitting artefacts from the core. **d**, **e** Directionality of the flaking sequence within the refit set. **f**, **g** Map and orientation of refit lines



Distances between conjoining pieces present a normal distribution, and are all ≤ 970 mm, with a mean of 475 mm (Table 1; Fig. 6c).

As shown in Fig. 5c, most Exp. 56 artefacts are clustered in a Rose diagram to the NE of the core, in a narrow range of 75° . This reduction sequence contains 18 stages,

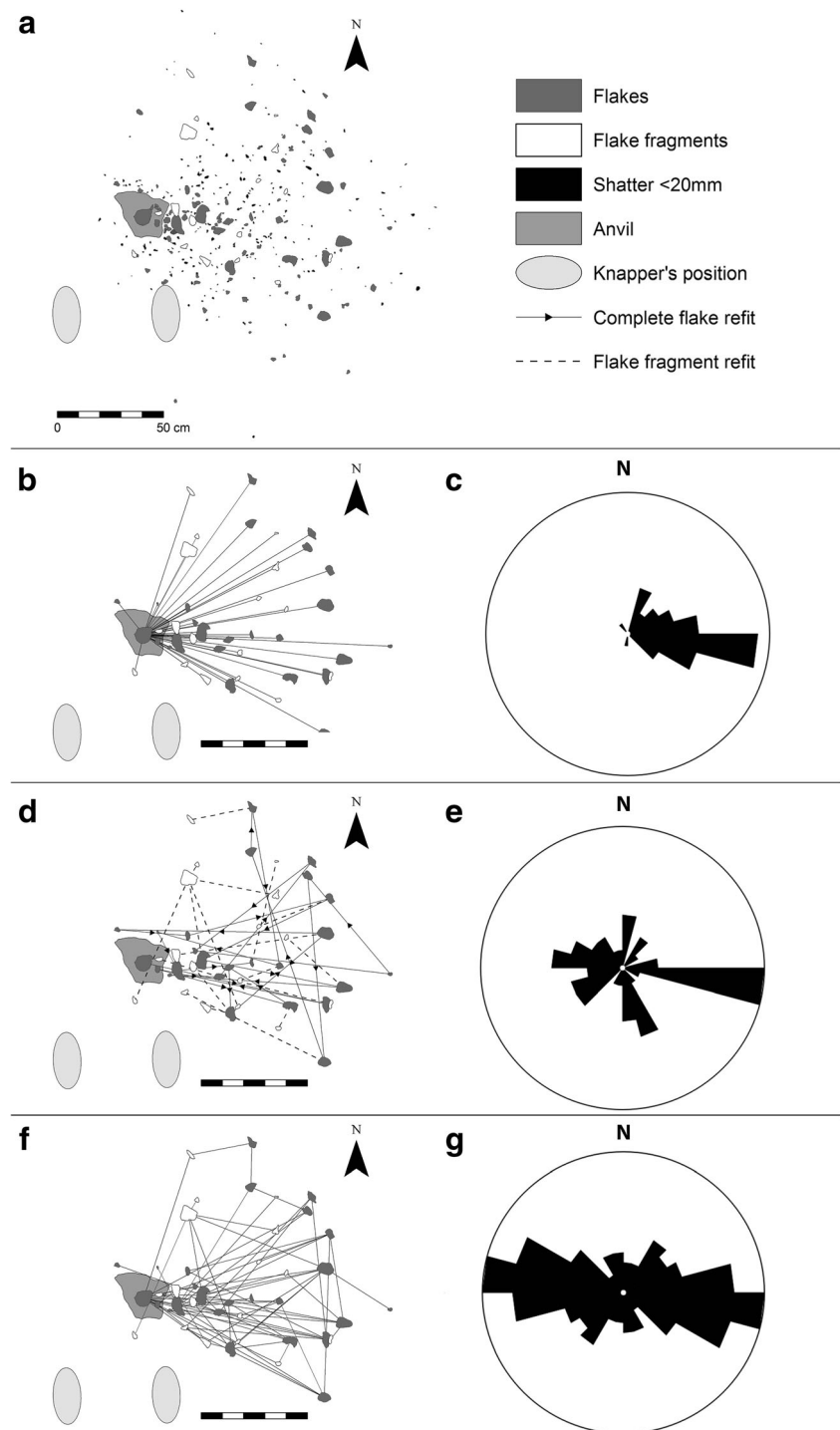
Fig. 3 Maps (**a**, **b**, **d**, **f**) and circular histograms (**c**, **e**, **g**) of Exp. 40. **a** All plotted artefacts. **b**, **c** Distribution of refitting artefacts from the core. **d**, **e** Directionality of the flaking sequence within the refit set. **f**, **g** Map and orientation of refit lines



where successive products are distributed randomly with respect to the previous detachment (Fig. 5d), with no pattern except a singular trend towards 240° – 255° . The

unimodal and symmetrical NE to SW distribution (Fig. 5g) may be linked to clustering near the anvil. On the other hand, one-to-one refit distances (mean =

Fig. 4 Maps (**a**, **b**, **d**, **f**) and circular histograms (**c**, **e**, **g**) of Exp. 54. **a** All plotted artefacts. **b**, **c** Distribution of refitting artefacts from the core. **d**, **e** Directionality of the flaking sequence within the refit set. **f**, **g** Map and orientation of refit lines



467 mm; see Table 1) show a wider variation than the other experiments (Fig. 6c).

Cluster analysis

ANN results show that the average distance in all experiments is clearly lower than the average distance in a hypothetical random distribution, indicating that materials follow a

clustered distribution (likelihood higher than 99%; Table 2). This is supported by Global Moran's statistics and the Getis–Ord method, indicating a dominance of high-concentration clusters. Ripley's K Function shows that clustering is maintained up to a distance of 1384–1396 mm, beyond which a dispersed pattern dominates (Table 2). Maximum clustering is reached at a distance of 380 mm for Exp. 18, and 464 mm for the rest of experiments.

Fig. 5 Maps (**a**, **b**, **d**, **f**) and circular histograms (**c**, **e**, **g**) of Exp. 56. **a** All plotted artefacts. **b**, **c** Distribution of refitting artefacts from the core. **d**, **e** Directionality of the flaking sequence within the refit set. **f**, **g** Map and orientation of refit lines

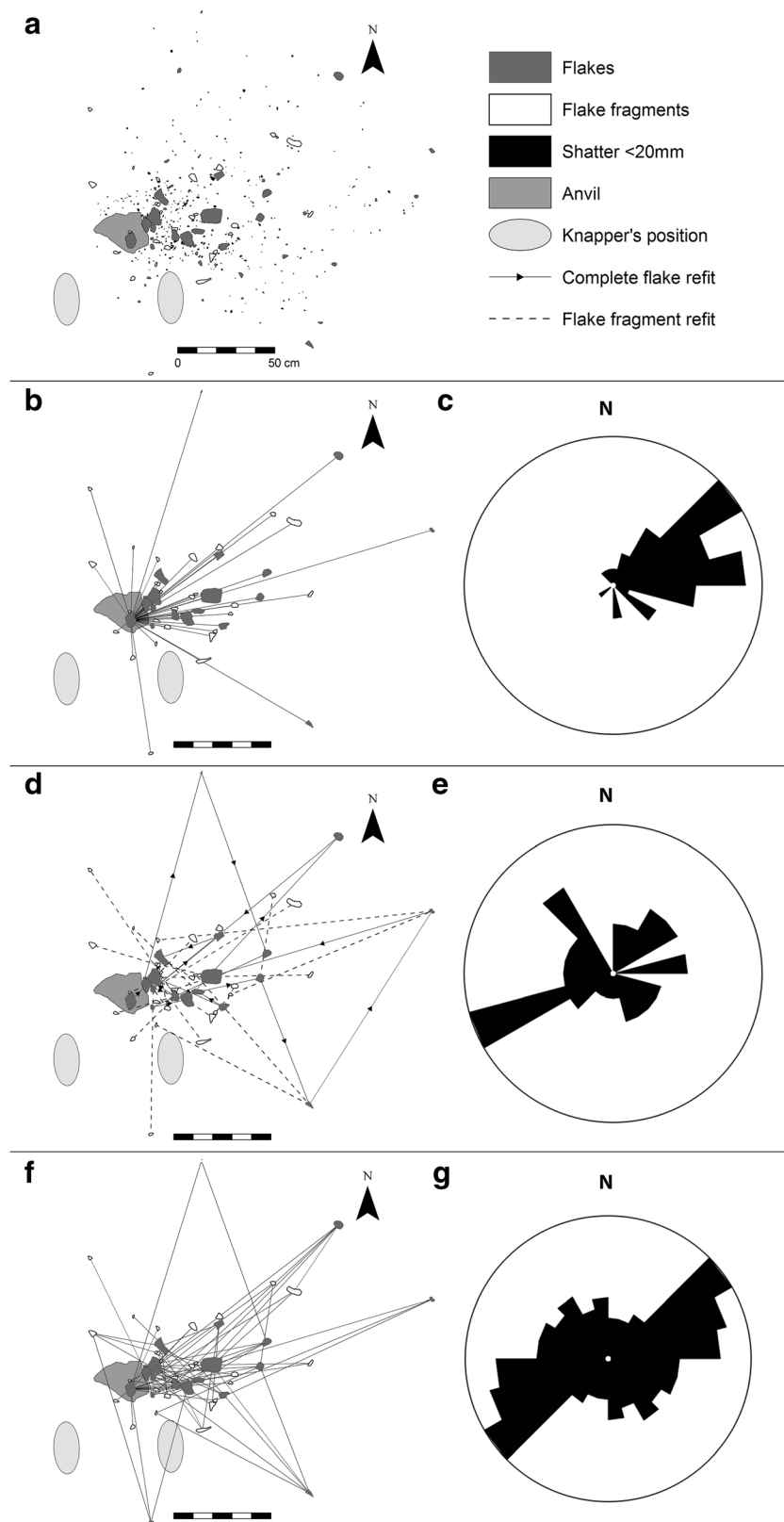
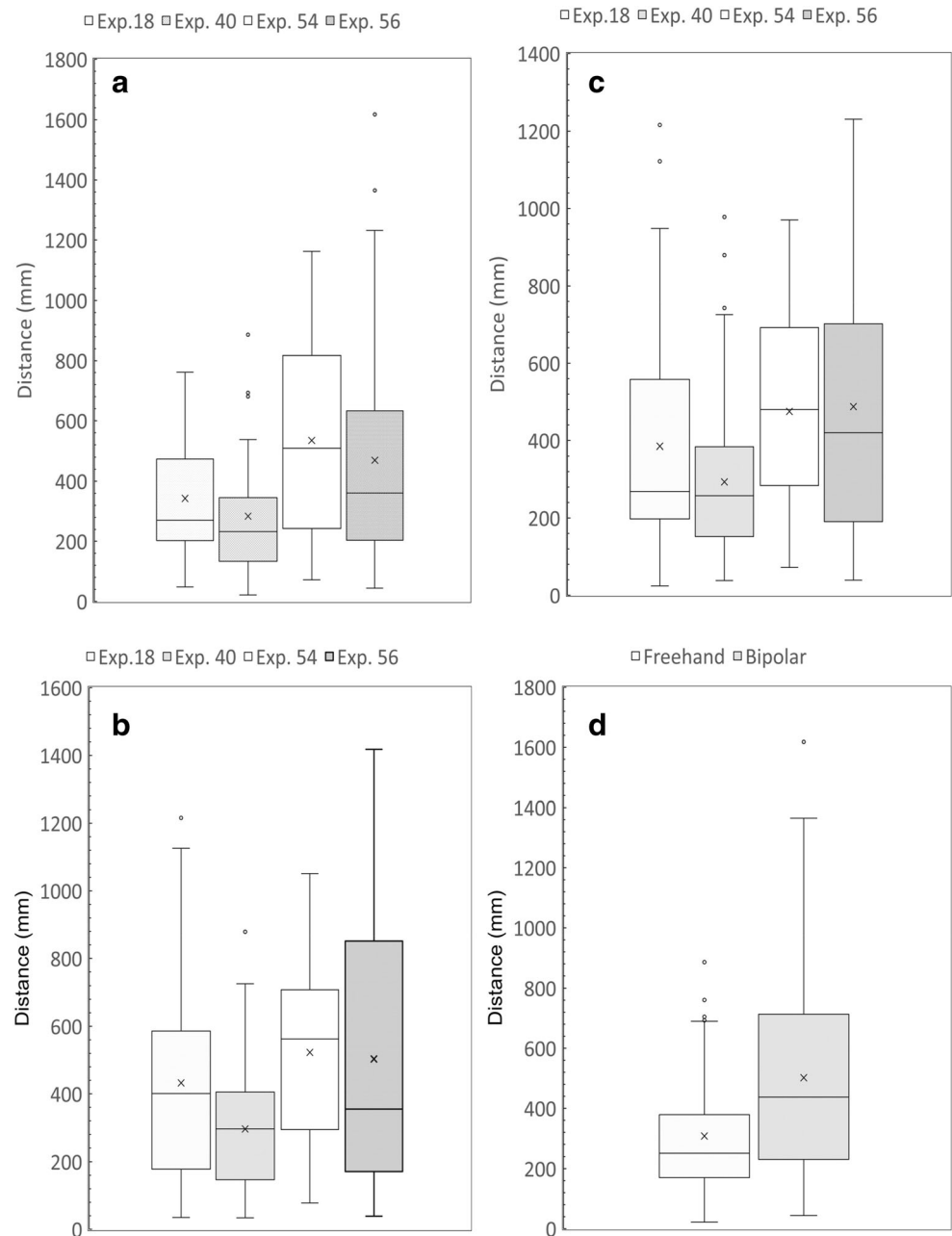


Figure 7 shows kernel maps of density and dispersion patterns of artefact frequency for each experiment. Exp. 18 has the lowest mean density, and Exp. 54 the highest mean density

(Table 3). Exp. 40 has the highest maximum density (0.08881), which determines the highest range of density data, with a standard deviation of 0.00891. Exp. 18 contains the

Fig. 6 Distances of **a** refitted artefacts to the core, **b** consecutive stages from the reduction sequence, **c** conjoining artefacts, **d** products to core



lowest maximum density (0.05862) and the lower standard deviation (0.00548; Table 3). This indicates that Exp. 54 and Exp. 56 share similar density patterns, whereas Exp. 18 and Exp. 40 have a higher variability and more extreme values. Dispersion of artefact frequency shows the highest concentration in front of the knapper for Exp. 40, and also in front, but slightly displaced to the right, for Exp. 18. Highest concentration areas can be clearly distinguished in the density maps (Fig. 7a), and are also detected as hot spot clusters by Gi* statistics with 95% level of confidence (Fig. 7b).

Both Exp. 18 and Exp. 40 also show an area of low artefact concentration that forms a distal arc from right to the left of the knapper. In Exp. 18, this low concentration area shows a

scattered pattern, whereas in Exp. 40 the low concentration area has a ring shape and is separated from the highest concentration area by a discontinuous strip with no material. Areas of low concentration do not constitute statistically significant cold spots, according to the Gi* method. The highest concentration areas in Exp. 54 and Exp. 56 are also defined by density maps and Gi* hotspots, and are strongly patterned to the right of the knapper.

Getis–Ord Gi* statistics (Fig. 7c, d) detected only hot spots or statistically significant concentrations of pieces with high length and weight values. For length, Exp. 18 and Exp. 40 show hot spots in front of the knapper which are very concentrated. Conversely, length patterns of Exp. 54 and Exp. 56 are

Table 2 Spatial pattern statistics of the experimental assemblages

	Exp. 18	Exp. 40	Exp. 54	Exp. 56
Average nearest neighbour (ANN)				
NN observed (mm)	37.59	41.49	39.14	32.47
NN expected (mm)	65.97	67.53	63.05	56.85
NN ratio	0.57	0.61	0.62	0.57
NN Z-score	− 14.39	− 12.61	− 13.28	− 16.65
<i>p</i> value	0	0	0	0
Ripley's K Function				
Clustered–dispersed change (mm)	1386	1384	1391	1394
Getis–Ord general G				
Observed general G	0.023	0.019	0.014	0.018
Expected general G	0.003	0.003	0.003	0.003
Z-score	19.635	19.900	19.923	19.854
<i>p</i> value	0	0	0	0
Global Moran's				
Moran's index	0.705	0.743	0.756	0.741
Expected index	− 0.003	− 0.003	− 0.003	− 0.003
Z-score	19.643	19.909	19.935	19.861
<i>p</i> value	0	0	0	0
Incremental global Moran's I				
Maximum peak (mm)	380	464	464	464
Distribution	Unimodal	Unimodal	Unimodal	Unimodal
Z-score	29.06	35.63	43.24	34.77

defined by hot spots to the right of the knapper, and show a more dispersed pattern, suggesting a higher dispersion of large pieces. This dual pattern is less obvious in the weight variable. Exp. 18 and Exp. 40 again show concentrated hot spots in front of the knapper, and Exp. 54 presents dispersed hot spots towards the right of the knapper. However, weight hot spots in Exp. 56 show a low dispersion: they are located to the right of the knapper, but are concentrated. Hot spot descriptive statistics show low values for Exp. 18 (Table 4), indicating the presence of smaller pieces in this assemblage; for example, hot spots reaching a 95% confidence include pieces with a mean length of 98–110 mm for Exp. 40, Exp. 54 and Exp. 56, but only of 67 mm for Exp. 18 (Table 4). Similarly, weight hot spots in Exp. 18 have a mean weight of 33 g and of 41–47 g for the other three experiments. No cold spots or statistically significant concentration of pieces with low length or weight were detected in any experiment.

Circular dispersion of conjoining sets

Core-to-flake displacements

Statistical tests of core-to-flake displacements show high statistical significance ($p < 0.01$) in all cases. This allows to reject the uniform distribution (Table 5) and indicates the presence of preferred orientations in the four experimental assemblages. Since

omnibus tests reject uniformity against unimodal and multimodal distributions, and the Rayleigh test detects only unimodal orientations, all the circular core-to-flake distributions can be essentially considered as unimodal preferred orientations.

The circular distribution of mean direction in the core-to-flake displacements of Exp. 18 and Exp. 40 indicates some significant differences (Fig. 8). While azimuths in Exp. 18 are mainly concentrated between 80 and 150° (Table 5), with a mean direction of 108.5° and a modal direction between 145 and 150°, the vectors in Exp. 40 are located mainly in the first quadrant, with a mean direction of 49.9° and a mode of 50–55° (Table 5). On the other hand, Exp. 54 and Exp. 56 display similar mean directions (83.5° and 67.2°, respectively), which overlap with 95% of confidence interval (Fig. 8). Their modal directions are also very similar (90–95° for Exp. 54 and 80–85° for Exp. 56, Table 5 and Fig. 8), and the dispersion of data (indicated by R and K) is higher than in Exp. 18 and Exp. 40. The most concentrated data is found in Exp. 54 ($R = 0.81$, $K = 2.99$), while Exp. 18 contains the highest dispersion ($R = 0.44$, $K = 0.97$).

Descriptive statistics also included weighting the displacement vectors with the distance covered by each piece from the core, and the artefact weight (Fig. 8a, Table 5). Results show that the mean direction does not vary significantly from the unfiltered data. Exp. 18 is where the mean changed the most significantly, varying close to 15° from weighted to unweighted data. On the other hand, the mean

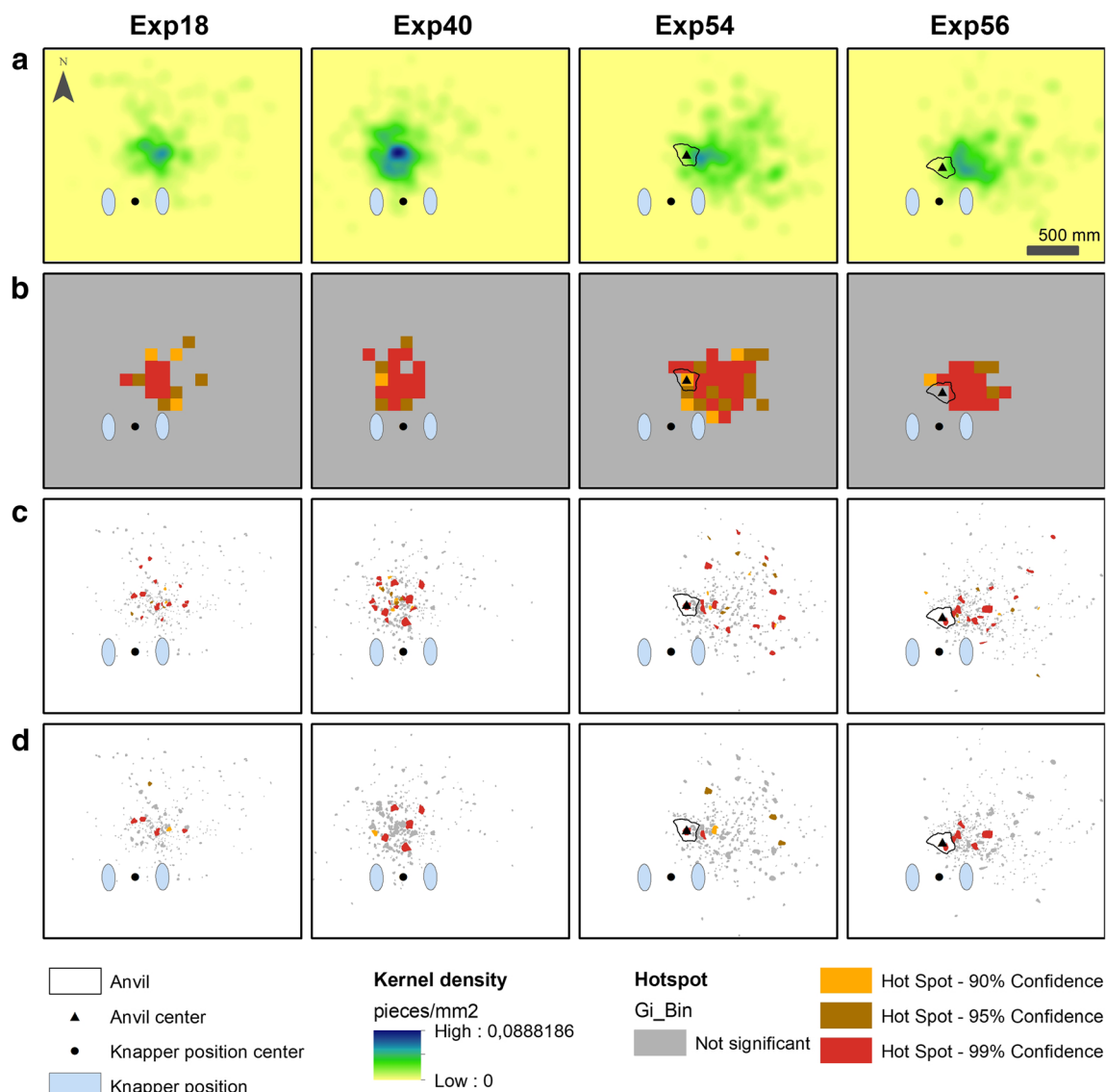


Fig. 7 Kernel density analysis and mapping of clusters using Getis–Ord Gi* statistics. **a** Kernel density maps. Results of Gi* statistics: **b** hot spots detected using the frequency of pieces (counting of pieces by quadrats of

125 mm) and inverse Euclidean distance. **c** Hot spots detected using piece length and inverse Euclidean distance. **d** Hot spots detected using piece weight and inverse Euclidean distance

direction did not change significantly in Exp. 54 and Exp. 56, which show variations of only 2–3°. The modal direction is more variable, but with no similar pattern shared by all experiments (Table 5). Regarding dispersion, weighted statistics show an increase of the concentration in all

experiments, excepting in the data weighted by the distance of Exp. 18, where the concentration is reduced slightly with respect to the unweighted statistics. In general, data weighted by artefact mass shows more concentrated parameters than data weighted by the distance, excepting in Exp. 56 (Table 5).

Table 3 Kernel density statistics of artefact maps

	Exp. 18	Exp. 40	Exp. 54	Exp. 56
Minimum	0	0	0	0
Maximum	0.05862	0.08881	0.05932	0.05393
Mean	0.00186	0.00287	0.00301	0.00249
SD	0.00548	0.00891	0.00686	0.00657

Refit lines

Clear differences in the axial data of refit lines exist between freehand and bipolar experiments. Statistical results of freehand knapping experiments do not allow rejecting the null hypothesis of uniformity with a >95% confidence interval. Minimum *p* values are obtained for Exp. 18, where Rayleigh's test and Rao's Spacing test only reach *p* = 0.073

Table 4 Hot spot descriptive statistics calculated for artefact frequency, size (i.e. artefact area) and weight, at 95% confidence interval

	Exp. 18	Exp. 40	Exp. 54	Exp. 56
Sample size (number of artefacts)				
Minimum	6	6	5	7
Maximum	27	16	12	24
Mean	12.4	9.7	7.4	12.8
SD	6.7	3.3	2	4.5
<i>n</i>	12	17	27	17
Area (mm ²)	187,500	265,625	421,875	265,625
Length (mm)				
Minimum	33.86	46.88	47.17	41.39
Maximum	67.50	100.74	98.51	110.14
Mean	47.65	68.40	66.33	63.59
SD	9.78	16.43	14.28	17.87
<i>n</i>	17	18	20	19
Weight (g)				
Minimum	367	1515	1013	1484
Maximum	2046	4290	7990	6548
Mean	943.67	2807.80	2698.40	2736.33
SD	543.23	1061.05	2680.38	1767.77
<i>n</i>	6	5	5	6

(92.7% confidence interval), and Exp. 40's statistical significance is even lower ($p > 0.15$). Therefore, no solid preferred orientation can be proposed for freehand knapping refit lines. Conversely, bipolar knapping data (Exp. 54 and Exp. 56) show high statistical significance for the Rayleigh test ($Z > 3.94$; $p < 0.019$) and demonstrate evidence of departure from uniformity in Rao's Spacing and Watson's omnibus tests ($0.025 < p < 0.005$; Table 5). These results suggest that bipolar refit lines show strong unimodal preferred orientations.

Refit mean directions are different within the freehand experiments (Exp. 18 = 130°, Exp. 40 = 32°; Table 5), whereas bipolar refit lines show more consistent mean directions, located around the 90–270° axis (axis 92–272° for Exp. 54 and axis 76–256° for Exp. 56). A similar—although weaker—relationship was observed in the refit line mode, which is more consistent within bipolar experiments than within freehand experiments (Table 5). The mode percentage is higher in bipolar (8–10.7%) than in freehand knapping (7.8%) (Table 5). The concentration parameters of refit lines also indicate a very dispersed distribution for Exp. 40 ($R = 0.11$ and $K = 0.22$) and the highest concentration for Exp. 54 ($R = 0.34$ and $K = 0.72$), while Exp. 18 and Exp. 56 have similar intermediate values. However, when refit lines are weighted by the distance (Fig. 8b), concentration similarities between Exp. 18 and Exp. 56 disappear, although they are still positioned between the end values of Exp. 40 and Exp. 54.

Discussion

Density patterns

Newcomer and de Sieveking (1980) investigated spatial patterns associated with knapper stance (e.g., standing, seated and sitting on the floor), and observed that the greater the distance from the floor, the larger and more diffused flaking scatters became (see also Fischer 1990). Schick (1984) employed a similar perspective and concurred with Newcomer and Sieveking (1980) that standing produced the largest and most diffuse lithic scatters, whilst also producing more elongated patterns whose density declined as the distance to the knapper increased. Lithic scatters produced whilst kneeling, squatting and sitting on the ground shared similar spatial patterning. These were all more densely clustered compared to standing and produced a more circular or oval distribution. Lithic spatial patterning according to varying reduction techniques has also been studied (e.g. Kvamme 1997) although, with the exception of Schick (1984)—who touched upon the spatial differences between freehand percussion and floor knapping; a position similar, but not identical, to bipolar knapping—to our knowledge freehand versus bipolar flaking had yet to be directly investigated.

Since proximity to the floor correlates with denser concentrations (Newcomer and de Sieveking, 1980; Schick 1984), it would be expected that bipolar flaking in Exp. 54 and Exp. 56 produced more tightly clustering patterns than freehand in Exp. 18 and Exp. 40. Whilst this may be the case for the smallest debris (whose spatial distribution is not the subject of our study), such an expectation is not entirely reproduced in our results, where > 20 mm pieces have a higher dispersion in bipolar than in freehand experiments (see Fig. 7). We propose this is due to the knapper's lack of control over the products during bipolar flaking; in freehand reduction, the detached product normally rests on the knapper's hand. However, the hand holding a bipolar core is not in contact with the flaking surface, and products often launch from the core and may travel longer distances from the knapping area, resulting in a more dispersed pattern.

Freehand versus bipolar knapping may also inform in spatial patterns of handedness, a subject that is starting to receive attention in the literature (e.g. Bargalló et al. 2017). As shown in Fig. 7, freehand scatters are largely centred with regard to the knapper's position, whereas the bipolar products are strongly biased towards the NE. Again, these distinctive patterns are associated with core manipulation; products in a freehand sequence are left by the knapper to drop vertically from the core, whereas in bipolar flaking the core's handling position blocks two quadrants, and products will land in the sectors associated with the hand that is manipulating the hammerstone. In the case of Exp. 54 and Exp. 56, produced by a right-handed knapper, artefact clusters will thus be located in the NE of the flaking area (Fig. 8).

Table 5 Circular statistics of refit orientations: (A) core-to-flake displacements (polar data); (B) refit lines (axial data)

	A				B			
	Exp. 18	Exp. 40	Exp. 54	Exp. 56	Exp. 18	Exp. 40	Exp. 54	Exp. 56
Variable	Azimuth	Azimuth	Azimuth	Azimuth	Axial	Axial	Axial	Axial
Number of observations (<i>n</i>)	36	48	41	45	64	90	75	80
Descriptive statistics								
No weighted data								
Mean vector, μ (°)	108.5	49.9	83.5	67.2	129.8	31.6	92.6	76.0
Length of mean vector, <i>R</i>	0.44	0.47	0.81	0.73	0.20	0.11	0.34	0.21
Modal direction (°)	145–150	50–55	90–95	80–85	130–135	50–55	100–105	65–70
Mode percentage (%)	11.1	8.3	12.2	11.1	7.8	7.8	10.7	8.0
Concentration, <i>K</i>	0.97	1.08	2.99	2.21	0.41	0.22	0.72	0.43
Weighted by distance								
Mean vector, μ (°)	93.7	46	81.1	67	145.2	45.8	90.8	68.5
Length of mean vector, <i>R</i>	0.40	0.62	0.86	0.78	0.32	0.13	0.38	0.243
Modal direction (°)	145–150	65–70	90–95	50–55	130–135	100–105	100–105	65–70
Mode percentage (%)	17.7	11.7	13.4	16.3	10.4	7.3	11.3	10.0
Concentration, <i>K</i>	0.89	1.60	3.82	6.71	0.68	0.26	0.83	0.50
Weighted by weight								
Mean vector, μ (°)	122.8	62.5	83.9	64.2				
Length of mean vector, <i>R</i>	0.46	0.70	0.89	0.92				
Modal direction (°)	105–110	115–120	100–105	70–75				
Mode percentage (%)	17.8	26.7	27.1	37.5				
Concentration, <i>K</i>	1.04	2.00	4.88	2.69				
Statistical tests								
Rayleigh test (<i>Z</i>)	6.8	10.7	26.9	23.9	2.612	1.029	8.669	3.945
Rayleigh test (<i>p</i>)	8.60E–04	1.26E–05	8.11E–12	6.15E–11	0.073	0.358	1.72E–04	0.019
Kuiper's test (uniform, <i>V</i>)	2.254	2.59	4.295	3.699	134.125	126	140.8	125.636
Kuiper's test (<i>p</i>)	< 0.01	< 0.01	< 0.01	< 0.01	0.50 > <i>p</i> > 0.10	0.90 > <i>p</i> > 0.50	0.50 > <i>p</i> > 0.10	0.90 > <i>p</i> > 0.50
Rao's spacing test (<i>U</i>)	167	169	226.317	194	0.152	0.073	0.475	0.23
Rao's spacing test (<i>p</i>)	< 0.01	< 0.01	< 0.01	< 0.01	0.1 > <i>p</i> > 0.05	0.5 > <i>p</i> > 0.25	< 0.005	< 0.025
Watson's <i>U</i> ² test (uniform, <i>U</i> ²)	0.407	0.605	1.566	1.362	1.401	1.074	2.358	1.98
Watson's <i>U</i> ² test (<i>p</i>)	< 0.005	< 0.005	< 0.005	< 0.005	> 0.15	> 0.15	< 0.01	< 0.025

Orientation patterns

The use of refit lines to address orientation patterns in archaeological assemblages is still uncommon and has been applied essentially to discuss post-depositional processes (e.g. Schick 1984; Austin et al. 1999; Pope 2002; Ashton et al. 2005; Sisk and Shea 2008; Santamaría et al. 2010; de la Torre et al. 2014; de la Torre and Wehr 2018; Deschamps and Zilhão 2018). Since the preferred orientation of archaeological remains is a strong indicator of hydraulic disturbance (e.g. Toots 1965; Isaac 1967; Schick 1984; Lenoble and Bertran 2004; Benito-Calvo and de la Torre 2011), the underlying assumption in the literature has been that orientation of refit lines should—like the main axis of individual artefacts—inform on the current direction.

While we do not wish to challenge this assumption, results presented in this paper enable us to introduce a cautionary note. Our analysis of refit orientations shows that, in a pristine setting, strongly preferred orientations are to be expected for core-to-flake displacements in bipolar and freehand knapping scenarios, and for refit lines in bipolar knapping episodes. In the case of freehand knapping episodes, refit lines produce random distributions or weakly orientated patterns. Therefore, in archaeological contexts with good conditions of preservation, knapping episodes may produce circular histograms of refit lines that, albeit strongly orientated in some cases, are unrelated to post-depositional disturbance. Thus, there appears to be a degree of equifinality in the use of Rose diagrams for refit lines since they may indicate either flow direction/slope processes in water/gravity-disturbed

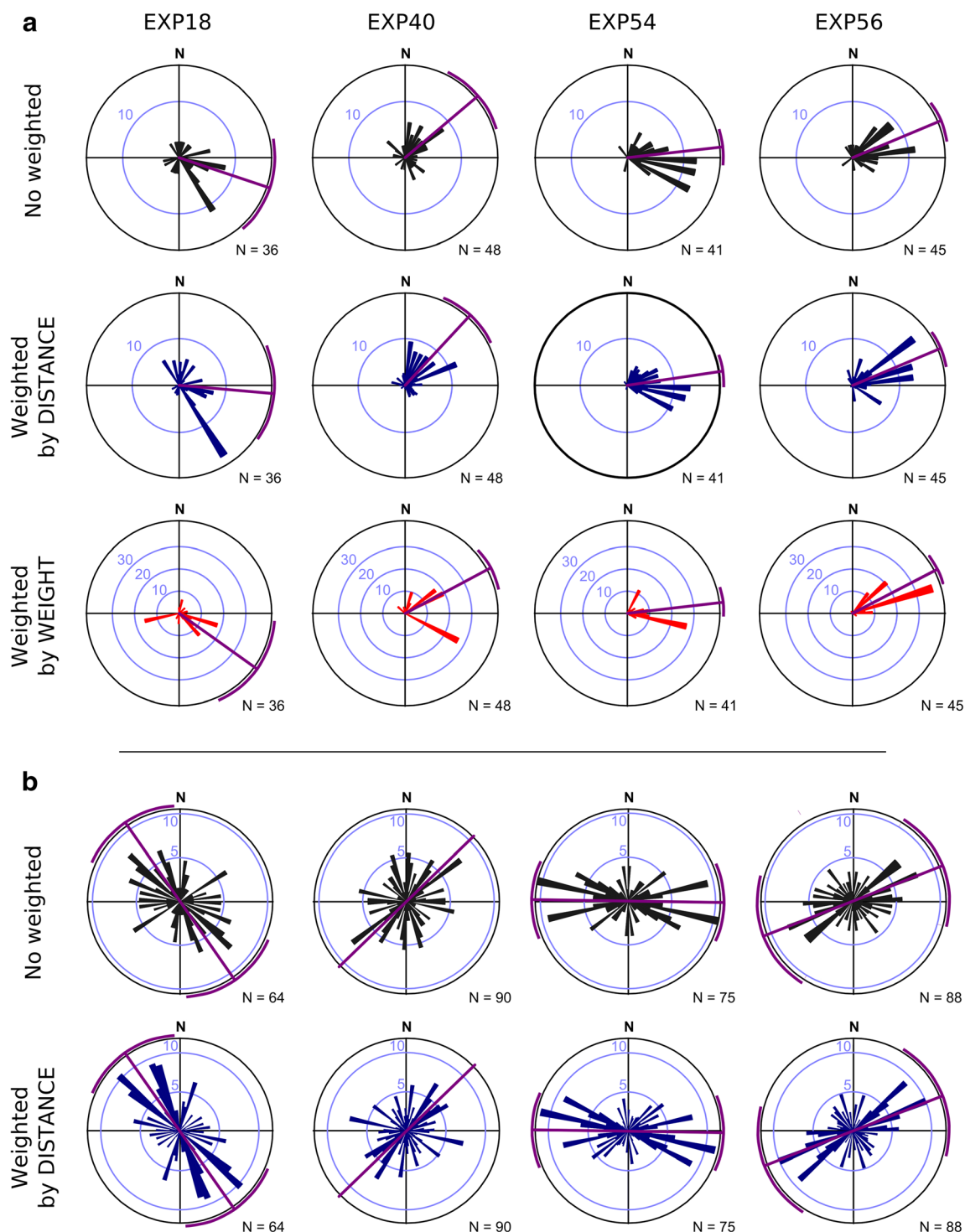


Fig. 8 Circular histograms of refit orientations, considering unfiltered data (i.e. no weighting), data weighted by distance and weighted by weight. **a** Histograms of core-to-flake displacements (polar data). **b** Histograms of refit lines (axial data)

assemblages or, quite on the contrary, the very position of the knapper in pristine sites. Therefore, results should be considered in the context of other proxies to achieve an accurate understanding of site formation processes.

Apart from acknowledging the reduced sample analysed here (limited to four experiments), it should also be stressed

that our experimental models are reductionist and do not account for the near-infinite number of variables that may affect the dispersion of artefacts and therefore the refit line circular histograms. From the dynamic position of the knapper, the fragmentation of the reduction sequences, to the use life of the artefact, many factors will have an influence on the Rose

diagrams of refit sets in real archaeological contexts. Despite these caveats, however, our results indicate that patterning exists in refit line orientations of some types of knapping episodes. Therefore, the analysis of circular histograms bears heuristic potential to make high-resolution interpretations of spatial dynamics, particularly in near-pristine sites (e.g. Pigeot 1990; Bodu et al. 1990; Vaquero et al. 2001; Roberts and Parfitt 1999), where preferential orientations may be used to investigate activity areas and micro-spatial patterns.

Conclusions

The identification of single knapping episodes in the Palaeolithic record (e.g. Pigeot 1990; Fischer 1990; Bodu et al. 1990; Pope 2002) makes it relevant to model the distribution of experimental assemblages and reconstruct their spatial dynamics. With the aid of GIS techniques, we have shown in this paper that knapping scatters have clustered distributions, with high concentrations across low-density areas. These spatial dynamics seem to be patterned, and therefore it might be possible to use density models to explore aspects such as handedness and flaking methods in the archaeological record.

Refit patterns in our experiments show that most conjoins are of short distances, most within less than half a meter radius of the knapper's position. While this is only to be expected in knapping episodes where no transport of tools is made, our analysis has also interesting results concerning the preferential orientation of refit lines. Preferential orientation of artefacts is a strong indicator of post-depositional disturbance, and circular histograms of refit connections have been used to address the extent of taphonomic processes (e.g. Austin et al. 1999; Ashton et al. 2005; de la Torre and Wehr, 2018; Deschamps and Zilhão, 2018). However, our results show that, perhaps counterintuitively, preferential orientation of refit lines is the common pattern in pristine flaking scatters associated to bipolar knapping. Although these results introduce some degree of equifinality on the interpretation of Rose diagrams for refit lines, they also highlight the potential of applying orientation analysis to refit studies, which can contribute high-resolution data on spatial dynamics of conjoining sets in Palaeolithic assemblages.

Acknowledgements We are grateful to Francesca Romagnoli and Manuel Vaquero for their invitation to participate in the workshop that led to the publication of this special issue. The workshop 'The Big Puzzle 30 years after: a multidisciplinary, shared, Palaeolithic perspective' was kindly supported by the Wenner-Gren Foundation Ref: Gr CONF-737. We are also thankful to the volunteers of the UCL-Lithics Lab that helped in processing the experiments. T. Proffitt's contribution was funded by a British Academy Fellowship (#542133). Raw material collection at Olduvai Gorge was funded by the European Research Council (Starting Grants 283366).

Open Access This article is distributed under the terms of the Creative Commons Attribution 4.0 International License (<http://creativecommons.org/licenses/by/4.0/>), which permits unrestricted use, distribution, and reproduction in any medium, provided you give appropriate credit to the original author(s) and the source, provide a link to the Creative Commons license, and indicate if changes were made.

References

- Ashton N, Lewis S, Parfitt S, Whittaker J, Candy I, Kemp R, Keen D, Penkman K, Thomas G, White MJ (2005) Excavations at the lower Palaeolithic site at Elveden, Suffolk, UK. *Proceedings Prehistoric Soc* 7:1–61
- Austin, L.A., Bergman, C.A., Roberts, M.B., Wilhelmsen, K.H., 1999. Archaeology of excavated areas, In: Roberts, M.B., Parfitt, S.A. (Eds.), Boxgrove. A Middle Pleistocene hominid site at Eartham Quarry, Boxgrove, West Sussex. English Heritage, London, pp. 309–426
- Bargalló A, Mosquera M, Lozano S (2017) In pursuit of our ancestors' hand laterality. *J Hum Evol* 111:18–32
- Barton RNE, Bergman CA (1982) Hunters at Hengistbury: some evidence from experimental archaeology. *World Archaeol* 14:237–248
- Benito-Calvo A, Martínez-Moreno J, Jordá Pardo JF, de la Torre I, Mora R (2009) Sedimentological and archaeological fabrics in Palaeolithic levels of the south-eastern Pyrenees: Cova gran and Roca dels Bous sites (Lleida, Spain). *J Archaeol Sci* 36:2566–2577
- Benito-Calvo A, Martínez-Moreno J, Mora R, Roy M, Roda X (2011) Trampling experiments at Cova gran de Santa Linya, pre-Pyrenees, Spain: their relevance for archaeological fabrics of the upper-middle Paleolithic assemblages. *J Archaeol Sci* 38:3652–3661
- Benito-Calvo A, de la Torre I (2011) Analysis of orientation patterns in Olduvai bed I assemblages using GIS techniques: implications for site formation processes. *J Hum Evol* 61:50–60
- Bertran P, Beauval C, Boulogne S, Brenet M, Costamagno S, Feuillet T, Laroulandie V, Lenoble A, Malaurent P, Mallye J-B (2015) Experimental archaeology in a mid-latitude periglacial context: insight into site formation and taphonomic processes. *J Archaeol Sci* 57:283–301
- Bodu P, Karlin C, Ploux S (1990) Who's who? The Magdalenian flintknappers of Pincevent (France). In: Czesla E, Eickhoff S, Arts N, Winter D (eds) The big puzzle: international symposium on refitting stone artefacts, Monrepos 1987. Holos, Bonn, pp 143–163
- Bordes, J.-G., 2003. Lithic taphonomy of the Châtelperronian/Aurignacian interstratifications in Roc de Combe and Le Piage (Lot, France). In: Zilhao, J., d'Errico, F. (Eds.), The chronology of the Aurignacian and the transitional technocomplexes. Dating, stratigraphies, cultural implications. IPA, Lisboa, pp. 223–244
- Boschian G, Saccà D (2010) Ambiguities in human and elephant interactions? Stories of bones, sand and water from Castel di Guido (Italy). *Quat Int* 214:3–16
- Bowers PM, Bonnicksen R, Hoch DM (1983) Flake dispersal experiments: noncultural transformation of the archaeological record. *Am Antiq* 48:553–572
- Byrne F, Proffitt T, Arroyo A, de la Torre I (2016) A comparative analysis of bipolar and freehand experimental knapping products from Olduvai Gorge, Tanzania. *Quat Int* 424:58–68
- Cahen D (1980) Question de contemporanéité: L'apport des remontages. *Bulletin de la Société Préhistorique Française* 77:230–232
- Czesla E (1990) On refitting of stone artefacts. In: Czesla E, Eickhoff E (eds) The big puzzle: international symposium on refitting stone artefacts. Verlag Bonn, Holos, pp 9–44
- de Loecker D, Kolen J, Roebroeks W, Hennekens P (2003) A refitter's paradise: on the conjoining of artefacts at Maastricht-Belvédère (the

- Netherlands). In: Moloney N, Shott MJ (eds) *Lithic analysis at the millennium*. Institute of Archaeology, UCL, London, pp 113–136
- de la Torre I, Benito-Calvo A (2013) Application of GIS methods to retrieve orientation patterns from imagery: a case study from beds I and II, Olduvai Gorge (Tanzania). *J Archaeol Sci* 40:2446–2457
- de la Torre I, Mora R, Arroyo A, Benito-Calvo A (2014) Acheulean technological behaviour in the middle Pleistocene landscape of Mieso (east-Central Ethiopia). *J Hum Evol* 76:1–25
- de la Torre I, Wehr, K., 2018. Site formation processes of the early Acheulean assemblage at EF-HR (Olduvai Gorge, Tanzania). *J Hum Evol* 120:298–328
- Deschamps M, Zilhão J (2018) Assessing site formation and assemblage integrity through stone tool refitting at Gruta da Oliveira (Almonda karst system, Torres Novas, Portugal): a middle Paleolithic case study. *PLoS One* 13:e0192423
- Driscoll K, Alcaina J, Égüez N, Mangado X, Fullola J-M, Tejero J-M (2016) Trampled under foot: a quartz and chert human trampling experiment at the Cova del Parco rock shelter, Spain. *Quat Int* 424: 130–142
- Fischer A (1990) A late Palaeolithic ‘school’ of flint-knapping at Trollesgave, Denmark. Results from refitting. *Acta Archaeologica* 60:33–49
- Fisher NI (1995) *Statistical analysis of circular data*. Cambridge University Press, Cambridge
- Gifford-González DP, Damrosch DB, Damrosch DR, Pryor J, Thunen RL (1985) The third dimension in site structure: an experiment in trampling and vertical dispersal. *Am Antiq* 50:803–818
- Hay RL (1976) *Geology of the Olduvai Gorge*. University of California Press, Berkeley
- Hiscock P (1986) The conjoin sequence diagram: a method of describing conjoin sets. *Queensland Archaeological Res* 3:159–166
- Hofman JL (1986) Vertical movement of artifacts in alluvial and stratified deposits. *Curr Anthropol* 27:163–171
- Isaac GL (1967) Towards the interpretation of occupation debris: some experiments and observations. *Kroeber Anthropological Soc Papers* 37:31–57
- Kreutzer LA (1988) Megafaunal butchering at Lubbock Lake, Texas: a taphonomic reanalysis. *Quat Res* 30:221–231
- Kvamme KL (1997) Patterns and models of Debitage dispersal in percussion flaking. *Lithic Technol* 22:122–138
- Lenoble A, Bertran P (2004) Fabric of Palaeolithic levels: methods and implications for site formation processes. *J Archaeol Sci* 31: 457–469
- Lenoble A, Bertran P, Lacrampe F (2008) Solifluction-induced modifications of archaeological levels: simulation based on experimental data from a modern periglacial slope and application to French Palaeolithic sites. *J Archaeol Sci* 35:99–110
- McPherron SP (2018) Additional statistical and graphical methods for analyzing site formation processes using artifact orientations. *PLoS One* 13:e0190195
- Nagle JS (1967) Wave and current orientation of shells. *J Sediment Petrol* 37:1124–1138
- Newcomer M, de Sieveking G (1980) Experimental flake scatter-patterns: a new interpretative technique. *J Field Archaeol* 7:345–352
- Nielsen AE (1991) Trampling the archaeological record: an experimental study. *Am Antiq* 56:483–503
- Pigeot N (1990) Technical and social actors: flintknapping specialists and apprentices at Magdalenian Etiolles. *Archaeological Review from Cambridge* 9:126–141
- Pope, M.I., 2002. The significance of biface-rich assemblages: an examination of behavioural controls on lithic assemblage formation in the lower Palaeolithic. Unpublished PhD thesis, Southampton University
- Proffitt T, de la Torre I (2014) The effect of raw material on inter-analyst variation and analyst accuracy for lithic analysis: a case study from Olduvai Gorge. *J Archaeol Sci* 45:270–283
- Roberts MB, Parfitt SA (eds) (1999) *Boxgrove. A middle Pleistocene hominid site at Eartham quarry, Boxgrove, West Sussex*. English Heritage, London
- Sánchez-Romero L, Benito-Calvo A, Pérez-González A, Santonja M (2016) Assessment of accumulation processes at the middle Pleistocene site of Ambrona (Soria, Spain). Density and orientation patterns in spatial datasets derived from excavations conducted from the 1960s to the present. *PLoS One* 11:e0167595
- Santamaría D, Fortea J, de la Rasilla M, Martínez L, Martínez E, Cañaveras JC, Sánchez-Moral S, Rosas A, Estalrich A, García-Tabernero A, Lalueza-Fox C (2010) The technological and typological behaviour of a Neanderthal group from El Sidrón cave (Asturias, Spain). *Oxf J Archaeol* 29:119–148
- Schick, K.D., 1984. Processes of Palaeolithic site formation: an experimental study. Unpublished PhD thesis. University of California, Berkeley, Berkeley
- Sisk ML, Shea JJ (2008) Intrasite spatial variation of the Omo Kibish Middle Stone Age assemblages: artifact refitting and distribution patterns. *J Hum Evol* 55:486–500
- Texier JP, Bertran P, Coutard JP, Francou B, Gabert P, Guadelli JL, Ozouf JC, Plisson H, Raynal JP, Vivent D (1998) TRANSIT, an experimental archaeological program in periglacial environment: problem, methodology, first results. *Geoarchaeology* 13:433–473
- Toots H (1965) Random orientation of the fossils and its significance. *University Wyoming Contributions Geology* 4:59–62
- Vaquero M, Vallverdú J, Rosell J, Pastó I, Allué E (2001) Neandertal behavior at the middle Palaeolithic site of Abric Romaní, Capellades, Spain. *J Field Archaeol* 28:93–114
- Villa P (1982) Conjoinable pieces and site formation processes. *Am Antiq* 47:276–290
- Villa P (2004) Taphonomy and stratigraphy in European prehistory. *Before Farming* 2004(1):1–20
- Wendt J (1995) Shell directions as a tool in palaeocurrent analysis. *Sediment Geol* 95:161–186